Alexandria Engineering Journal (2022) xxx, xxx–xxx

HOSTED BY

Alexandria University

Alexandria Engineering Journal

www.elsevier.com/locate/aej
www.sciencedirect.com

ORIGINAL ARTICLE

Solutions and compatibility conditions for a model describing the interaction of gases in a fuel tank

José Luis Díaz Palencia, Julián Roa González, Isaac Seoane Pujol

Universidad a Distancia de Madrid, Spain

Received 13 August 2022; revised 8 October 2022; accepted 21 October 2022

KEYWORDS

Reaction - diffusion modeling;
Gas interaction;
Inerting;
Vented fuel tanks

Abstract The fire safety is a relevant problem in aircraft fuel tanks design. One of the most suitable solutions is based on the introduction of nitrogen, through distributed nozzles, to decrease the tank flammability. This is given by the nitrogen that pulls the oxygen outboard. There exist several models and solutions to describe the interaction of gasses in a fuel tank, nonetheless it is still missing to provide the compatibility conditions required to ensure an inerted ullage. Following this idea, the intention is to provide new results about the required conditions to ensure that the vented convection, given by the fuel tank venting system, does not impact the propagation of the nitrogen to construct an inerted airspace. We introduce some new flat solutions that complement those already existing in the literature. The flat solutions can be used to assess the time required to get an inerted fuel tank configuration in a direct way, representing a simplification on the calculation of the time-to-inert compared to that existing in the current literature. The analytical approaches are validated with real data extracted from a flight test campaign in an Airbus A320. We highlight that the obtained results fit quite exactly with the flight test data.

1. Introduction

A Boeing 747–131 property of the company Trans World Airlines crashed on July-1996 over the Atlantic Ocean. After and extensive investigation, it was concluded that the most probable origin of the explosion was a spark generated by a fuel pump in the centre wing tank. This was further aggravated due to the heat generated by the air conditioning packs, located in a zone close to the fuel tank.

As a design solution, to avoid similar occurrences, the safety aviation authorities proposed the installation of a Inerting System (see [1]) with the intention of removing the oxygen and replacing it by an inerted gas, as the nitrogen for example. The idea of introducing an inerted fuel tank ullage was not new at that moment. It had been previously conceived by the military aviation to reduce the battle damage, whenever a threat (for instance any high energy shrapnel) impacts the wing tanks with structural penetration.

It is universally accepted that the explosion risks are minimized when the oxygen concentration in a fuel tank ullage is

E-mail addresses: joseluis.diaz.p@udima.es (J.L. Díaz Palencia), julian.roa@udima.es (J.R. González), isaac.seoane@udima.es (I.S. Pujol)

Peer review under responsibility of Faculty of Engineering, Alexandria University.

https://doi.org/10.1016/j.aej.2022.10.055

below 9% for military applications and below 7% for civil aircrafts (> 93% of nitrogen).

Technically speaking, one of the most mature and optimal technology to produce an inerted ullage in an aircraft fuel tank, is based on the separation of the oxygen and nitrogen naturally presented in the air. This is achieved by the action of semipermeable fibers that are hosted in a canister of cylindrical shape known as Air Separation Module (ASM). The ASM contains ports and chambers to handle the Nitrogen Enriched Air (NEA) and the Oxygen Enriched Air (OEA) exhausts. The pressurized air comes from the engine bleed system and is well conditioned (pressure ant temperature controlled) previously to be introduced into the ASM fibers. The oxygen moves radially and is expelled outboard. The nitrogen flows through the filters axially and is introduced in the fuel tank through a set of nozzle distributed in the tank airspace.

Since the inerting system was firstly introduced, one of the main areas of research was the construction of mathematical models to understand the gases interaction, so that the inerted state can be foreseen. One of the most relevant models, used by the aircraft designers, is based on simple algebraic equations describing the rate of air going into the inerting system and the rates of oxygen and nitrogen going out (see [2] for further details). The authors in [3,4] introduced a model based on a mass balance between tank bays. The resulting model was discussed with purely algebraic techniques and with a hybrid of algebraic and differential approaches, supported by the transport equation. In both cases, the models did not introduce any diffusion principle. The first study introducing diffusion, to the knowledge of the authors, is provided in the reference [6], where the authors discussed the concentration of fuel vapors with a basic parabolic PDE. Herein, the spatial variable was considered as the vertical to the tank. In [5], an algorithm was proposed to determine the ullage oxygen concentration by the washing model, but removing the uncertainly in the selection of the initial derivatives for a stable and convergent method. In other occasions, the models were built based on experimental approaches. In this regards, the authors in [7,8] developed a procedure based on tests to determine the impact on the inerted state due to the air composition as a mixture of nitrogen, oxygen and carbon dioxide. Another interesting analysis was provided by Bae and Blosch in [9]. The authors tested the impact in the oxygen concentration due to the concentration gradients in the fuel tank. Following the works focused on tests, in [10], the author discussed some experiments to understand the level of reduced oxygen concentration to prevent fuel tank risks. Other different models were provided in [11–13]. Particularly, in [13], the authors provided a numerical method to determine the evolution of dissolved oxygen. In [14], a numerical analysis is introduced to understand the influence of the ambient pressure on the inerted status in an aircraft fuel tank. In other cases, some analysis have been conducted to model the temperature behaviour of pressurized cryogenic tanks by numerical means (see [17]).

A further sophisticated model was introduced in [15]. The driving equation considered the main physical principles involved in the interaction of gases: diffusion, reaction and forced convection because of the tank venting outboard. Nonetheless, at the moment of such a model proposal, it was not clear what conditions were required to ensure that the tank ventilation conditions (forced convection) does not detrimentally impact the other mechanisms consisting on diffusion and reaction. If any of the last mentioned principles are negligible, compared with the action of the forced convection, it could be the case that the nitrogen does not reach all the fuel tank locations. This is particularly relevant in aircraft fuel tanks with complex geometries involving different bays. The exact assessments of the mentioned conditions constitute an important novelty in our study. Certainly, we will state the new compatibility results to ensure that the inerted configuration is achieved. For this end, the postulated model is formulated with an integral representation, and such involved integrals are carefully solved and balanced.

There exist other studies in the literature dealing with relevant physical topics. One of this is related with the temperature stratification within a tank, that may impact the diffusive mechanism of any gas. In [16], the authors provide a reduced model to predict the temperature stratification by natural convection in a hydrogen tank. Other aspects, like slosh waves formation and droplets formation in fuel tanks, are analyzed in [18,19]. Eventually, we remark that another important phenomenon in fuel tanks is related with the fuel bubbles formation, that can induce fuel vapors impacting the inerting performance. Some interesting works in this regard are given in [20,21].

2. Model proposal

Preliminary, we can start by considering that the nitrogen concentration N, with $0 < N \leqslant 1$, increases over time while the oxygen concentration Θ, with $0 < \Theta \leqslant 1$, decreases accordingly. Mathematically speaking, both functions depart from a finite mass distribution, and given the close tank area, the solutions can be requested to belong to a general Lebesgue space, this is $N(x,t),\ \Theta(x,t) \in L^1(\mathbb{R}^3)$. Physically, this implies that each concentration is regarded as a controlled mass during the evolution. No blow up is expected neither globally nor locally in time.

For a complete discussion about the model derivation, the reader is referred to [15]. The model is partly reproduced here for the sake of convenience. The basic driving equation is given as:

$$\begin{aligned} N_t &= \delta \Delta N + a \cdot \nabla N - \Theta^n (N - r), \\ \Theta_t &= \epsilon \Delta \Theta + a \cdot \nabla \Theta - N^m \Theta, \\ & 0 < n, m < 1, \\ N_0(x), \Theta_0(x) &\in L^\infty(\mathbb{R}^3) \cap L^1_{loc}(\mathbb{R}^3), \end{aligned} \tag{1}$$

where $r \geqslant \max_{x \in \mathbb{R}^3}\{N_0(x)\}, a$ is the vented convection vector and n, m two constants to be calibrated in each particular application. The different involved parameters were obtained based on the data from a developed flight test as per [22] (see the reference [15] for the complete discussion about), so that:

$$\begin{aligned} & n = 0.586,\ \ m = 0.025,\ \ a = 0.0125 m/min, \\ & \delta = \epsilon = 0.196\ cm^2/s. \end{aligned} \tag{2}$$

It is worth quoting that these values have been obtained for a stabilized flight out of transitory flight conditions, like the take off, climbing or descending phases.

3. Summary of the main results

The following Theorems compile the main analytical results shown in the coming sections:

Theorem 1. Given the set of solutions $(N,\Theta)\in C^{2+\alpha,\,1+\alpha/2}\big(\mathbb{R}^3\times(0,T)\big),\alpha>0$, with $\Theta_t\leqslant 0$ and $N_t\geqslant 0$, some new compatibility conditions, involving the initial distributions, are shown to ensure that the reaction term predominates over the diffusion and the vented convection:

$$\Theta_0^n\geqslant 2a\cdot\nabla N_0,\quad \Theta_0^n\geqslant \delta\mid\nabla N_0\mid^2 2N_0,\quad \int_{\mathbb{R}^3}N_0^m\geqslant\mid a\mid\Theta_0.$$

In addition and for a stabilized flight, the diffusion predominates over the vented convection if the following holds:

$$\delta\nabla N_0\geqslant 2a\cdot\nabla N_0-\mid a\mid N_0.$$

Theorem 2. The following is a flat solution to the nitrogen concentration:

$$N(t)=\|N(x,0)\|_{L^1}+\theta t, \tag{3}$$

while a solutions for the oxygen concentration is given as:

$$\Theta(t)=\|\Theta(x,0)\|_{L^1}-\frac{1}{\theta(m+1)}\left(\|N(x,0)\|_{L^1}+\theta t\right)^{m+1}. \tag{4}$$

Both solutions are locally valid in $(0,T)$, where

$$T=\frac{\left(\|\Theta(x,0)\|_{L^1}-\theta^{1/n}\right)^{\frac{1}{m+1}}(\theta(m+1))^{\frac{1}{m+1}}-\|N(x,0)\|_{L^1}}{\theta}, \tag{5}$$

being $\theta>0$, the residual or terminal concentration of oxygen in the fuel tank airspace.

4. Proof, discussions and validation of Theorem 1

In this section, we provide a proof to the Theorem 1 together with some paramount discussions about the validation in a real flight scenario.

Proof. We start by considering the problem (1), so that after multiplication of the first equation by N^2, and the second by Θ^2, the following holds:

$$\begin{aligned}N_tN^2&=\delta\Delta NN^2+a\cdot\nabla NN^2-\Theta^n(N-r)N^2,\\ \Theta_t\Theta^2&=\epsilon\Delta\Theta\,\Theta^2+a\cdot\nabla\Theta\,\Theta^2-N^m\Theta^3.\end{aligned} \tag{6}$$

Making the integration in the domain $\mathbb{R}^3\times(0,T)$:

$$\begin{aligned}\int_{\mathbb{R}^3}\int_0^T N_tN^2&=\int_{\mathbb{R}^3}\int_0^T\delta\Delta NN^2\\&\quad+\int_{\mathbb{R}^3}\int_0^T a\cdot\nabla NN^2+\int_{\mathbb{R}^3}\int_0^T\Theta^n(r-N)N^2,\end{aligned} \tag{7}$$

$$\begin{aligned}\int_{\mathbb{R}^3}\int_0^T\Theta_t\Theta^2&=\int_{\mathbb{R}^3}\int_0^T\epsilon\Delta\Theta\Theta^2\\&\quad+\int_{\mathbb{R}^3}\int_0^T a\cdot\nabla\Theta\Theta^2-\int_{\mathbb{R}^3}\int_0^T N^m\Theta^3.\end{aligned} \tag{8}$$

The idea now is to develop further each of the involved integrals. The following ones are assessed by standard techniques:

$$\int_{\mathbb{R}^3}\int_0^T\delta\Delta NN^2=\int_0^T\delta N^2\mid\nabla N\mid-\int_{\mathbb{R}^3}\int_0^T\delta\mid\nabla N\mid^2 2N, \tag{9}$$

$$\int_{\mathbb{R}^3}\int_0^T a\cdot\nabla NN^2=\int_0^T\mid a\mid N^3-\int_{\mathbb{R}^3}\int_0^T N2Na\cdot\nabla N. \tag{10}$$

Operating in a similar basis for the equation in Θ:

$$\int_{\mathbb{R}^3}\int_0^T\epsilon\Delta\Theta\Theta^2=\int_0^T\epsilon\Theta^2\mid\nabla\Theta\mid-\int_{\mathbb{R}^3}\int_0^T\epsilon\mid\nabla\Theta\mid^2 2\Theta, \tag{11}$$

$$\int_{\mathbb{R}^3}\int_0^T a\cdot\nabla\Theta\Theta^2=\int_0^T\mid a\mid\Theta^3-\int_{\mathbb{R}^3}\int_0^T\Theta 2\Theta\, a\cdot\nabla\Theta. \tag{12}$$

Returning to (7) and (8), with the assessments done, the following holds:

$$\begin{aligned}&\textstyle\int_{\mathbb{R}^3}\int_0^T N_tN^2=\int_0^T\delta N^2\mid\nabla N\mid-\int_{\mathbb{R}^3}\int_0^T\delta\mid\nabla N\mid^2 2N\\&\textstyle+\int_0^T\mid a\mid N^3-\int_{\mathbb{R}^3}\int_0^T N2Na\cdot\nabla N+\int_{\mathbb{R}^3}\int_0^T\Theta^n(r-N)N^2\\&\textstyle\geqslant\int_{\mathbb{R}^3}\int_0^T\Theta^n(r-N)N^2-\int_{\mathbb{R}^3}\int_0^T\Big(\delta\mid\nabla N\mid^2 2N+N2Na\cdot\nabla N\Big).\end{aligned} \tag{13}$$

The observation, of the involved physics in a real scenario, leads to consider an increasing function N with time, this is $N_t\geqslant 0$. Then, it shall be required that:

$$\Theta^n(r-N)N^2\geqslant\delta\mid\nabla N\mid^2 2N+N2Na\cdot\nabla N. \tag{14}$$

Making the same operations for the equation in Θ, the following holds:

$$\begin{aligned}\textstyle\int_{\mathbb{R}^3}\int_0^T\Theta_t\Theta^2&\textstyle=\int_0^T\epsilon\Theta^2\mid\nabla\Theta\mid-\int_{\mathbb{R}^3}\int_0^T\epsilon\mid\nabla\Theta\mid^2 2\Theta\\&\textstyle+\int_0^T\mid a\mid\Theta^3-\int_{\mathbb{R}^3}\int_0^T\Theta 2\Theta\, a\cdot\nabla\Theta-\int_{\mathbb{R}^3}\int_0^T N^m\Theta^3\\&\textstyle\leqslant\int_0^T\epsilon\Theta^2\mid\nabla\Theta\mid+\int_0^T\mid a\mid\Theta^3-\int_{\mathbb{R}^3}\int_0^T N^m\Theta^3.\end{aligned} \tag{15}$$

The removal of the oxygen in the tank airspace leads to consider $\Theta_t\leqslant 0$, which implies to have:

$$\int_0^T\epsilon\Theta^2\mid\nabla\Theta\mid+\int_0^T\mid a\mid\Theta^3-\int_{\mathbb{R}^3}\int_0^T N^m\Theta^3\leqslant 0. \tag{16}$$

In summary, our idea is to determine the required conditions so that the expressions (14) and (16) are achieved. To this end, consider first the following inequality focused on the advection term:

$$\Theta^nN^2\geqslant\frac{\delta\mid\nabla N\mid^2 2N+N2Na\cdot\nabla N}{r-N}\geqslant\frac{N2Na\cdot\nabla N}{r-N}. \tag{17}$$

Proceeding similarly, the following inequality holds for the diffusive term related with the nitrogen gas:

$$\Theta^nN^2\geqslant\frac{\delta\mid\nabla N\mid^2 2N+N2Na\cdot\nabla N}{r-N}\geqslant\frac{\delta\mid\nabla N\mid^2 2N}{r-N}. \tag{18}$$

It should be noted that the last inequalities compare the vented convection with the reaction term (17), and the reaction term with the diffusion (18). Then, the following conditions hold:

$$\Theta^n\geqslant\frac{2a\cdot\nabla N}{r-N},\quad \Theta^n\geqslant\frac{\delta\mid\nabla N\mid^2 2N}{(r-N)N} \tag{19}$$

Now, for the equation in Θ:

$$\int_{\mathbb{R}^3}\int_0^T N^m\Theta^3\geqslant\int_0^T\epsilon\Theta^2\mid\nabla\Theta\mid+\int_0^T\mid a\mid\Theta^3, \tag{20}$$

so that

$$\int_{\mathbb{R}^3} N^m\Theta^3 \geqslant \epsilon\Theta^2 \mid \nabla\Theta \mid + \mid a \mid \Theta^3 \geqslant \mid a \mid \Theta^4. \tag{21}$$

Note that for this last expression, we recall that the volumetric concentration for the oxygen is assumed to be $0 < \Theta \leqslant 1$. The calculation for the involved integral in the previous expression is considered over a mean value of Θ. Then, it holds that:

$$\int_{\mathbb{R}^3} N^m \geqslant \mid a \mid \Theta. \tag{22}$$

Now, in return to the expression (13), it is possible to derive a condition to compare the diffusive term with the vented advection while keeping the condition $N_t \geqslant 0$. To this end, it suffices to take:

$$\delta N^2\nabla N + \mid a \mid N^3 \geqslant 2N^2 a\cdot\nabla N, \quad \delta\nabla N \geqslant 2a\cdot\nabla N - \mid a \mid N. \tag{23}$$

The results obtained in (19), (22) and (23) are applicable to any arbitrary small T, including as well the initial distributions. In addition, we can select a value of r such that $0 < r - N_0 < 1$. Recall that any concentration is such that: $0 < N < 1$, then it suffices to consider $r = 1$. Then:

$$\Theta_0^n \geqslant 2a\cdot\nabla N_0, \quad \Theta_0^n \geqslant \delta \mid \nabla N_0\mid^2 2N_0, \quad \int_{\mathbb{R}^3} N_0^m \geqslant \mid a \mid \Theta_0, \quad \delta\nabla N_0 \geqslant 2a\cdot\nabla N_0 - \mid a \mid N_0. \tag{24}$$

End of proof.

The initial distributions to be considered are given by the well-known oxygen and nitrogen mixture in the atmosphere. In a simplify, but sufficiently accurate, approach, we can consider that the air is formed of 80% of nitrogen ($N_0 = 0.8$) and 20% of oxygen ($\Theta_0 = 0.2$). Then $\nabla N_0 = 0$, therefore we have:

$$\Theta_0^n \geqslant 2a\cdot\nabla N_0 = 0, \quad \Theta_0^n \geqslant \delta \mid \nabla N_0\mid^2 2N_0 = 0. \tag{25}$$

Note that $\Theta_0^n = 0.2^{0.586} = 0.389$ (refer to [15] for a determination of the value of n). The first and second compatibility conditions are hence met as $0.389 > 0$.

Considering, now, the third compatibility condition, we should firstly describe the volume of integration given by an aircraft fuel tank. To this end, we consider the centre wing box of an Airbus A320, as the data collected for validation purposes are based on the reference [22]. Nonetheless, in the opinion of the authors, the same dynamics can be made applicable to any other larger fuel tank, as the scaling principles between geometry and design, to produce an inerted configuration, are normally preserved.

The centre wing tank, of a typical civil aircraft, is hosted in the aft zone to the forward cargo compartment, and is located in a forward area to the main landing gear. Approximately, the A320 centre wing tank can be understood as a box of dimensions: 4.5 m wide, 5 m long and 1.2 m as mean height. For another aircraft, like a Boeing 747, a set of typical tank dimensions are: 6.5 m wide, 6 m long and 1.5 m as mean height.

Then, the following calculations hold for the third compatibility condition:

$$\int_{A320\,tank} N_0^m\,dV = 0.80^{0.025}\,V_{A320\,tank} = 0.80^{0.025}\cdot 1.2\cdot 5\cdot 4.5 = 26.85,$$
$$\int_{B747\,tank} N_0^m\,dV = 0.80^{0.025}\,V_{B747\,tank} = 0.80^{0.025}\cdot 1.5\cdot 6\cdot 6.5 = 58.17. \tag{26}$$

The reader is referred to [15] for the value of $m = 0.025$.

In addition, we have $\mid a \mid \Theta_0 = 0.0125\cdot 0.2 = 0.0025$ (for an assessment of the value of $\mid a \mid$ refer to [15]). Then: $\int_{tank} N_0^m\,dV > \mid a \mid \Theta_0$ for both tanks.

Eventually, the fourth compatibility condition, that expresses a predominant diffusion over the vented convection in a stabilized flight, requires:

$$\delta\nabla N_0 \geqslant 2a\cdot\nabla N_0 - \mid a \mid N_0 \to 0 \geqslant -0.014\cdot 0.8, \tag{27}$$

which is indeed met.

We should notice henceforth that the compatibility conditions are met. Then, it is possible to conclude that the vented convection is relatively weak compared with the reaction and diffusion terms given in each equation for N and Θ. This allows us to consider that the nitrogen increases over time homogeneously in all fuel tank locations ($N_t(t) > 0$ with $\Theta_t(t) < 0$), even in zones of complicated geometry. In such zones, the gas motion is driven mainly by the diffusion that is pulled out by the governing reaction.

5. Proof, discussions and validation of Theorem 2

Now, the idea is to make use of the monotone behaviour of the reaction/absorption terms in (1) to obtain a precise assessment of solutions and to determine their order of growth. Particularly, we are interested on exploring a nondecreasing lower solution for the nitrogen concentration N ($N_t \geqslant 0$) and a nonincreasing upper solution for the oxygen concentration Θ ($\Theta_t \leqslant 0$). The rationale of this new objective is exposed as follows:

The governing Eq. (1) was initially proposed with the intention of finding the evolution of both, the concentrations of nitrogen and oxygen, to prevent a potential fuel tank ignition. The calculation of a lower solution for the nitrogen, and a upper solution for the oxygen, will lead to an underestimation of the concentration of nitrogen and a overestimation of the oxygen one at any $t > 0$. These approaches are valid for our intention, as they are conservative enough. Indeed, assume that locally in time, the lower nitrogen solution and the upper oxygen solution lead to a potential flammable condition, in case of a spark occurs within the fuel tank. Hence, it is required to wait for increasingly time values, so that at a higher local time the under-estimation of nitrogen reaches the required threshold of 93% in the fuel tank ullage to avoid potential explosions.

Before the calculation of the upper and lower solutions, we need the following supporting lemma:

Lemma 1. Assume an arbitrary $\Upsilon \in \mathbb{R}^+$, satisfying

$$0 < \Upsilon < \min_{x\in\mathbb{R}^3}(N(x,0),\Theta(x,0)). \tag{28}$$

The initial distributions are then rewritten as:

$$N(x,0)+\Upsilon,\ \Theta(x,0)+\Upsilon,\ N(x,0)-\Upsilon,\ \Theta(x,0)-\Upsilon. \tag{29}$$

The following solutions take on from the observed intial distributions

$$(N(x,0)+\Upsilon,\Theta(x,0)+\Upsilon) \to \left(\widehat{N}_\Upsilon(x,t),\hat{\Theta}_\Upsilon(x,t)\right),$$
$$(N(x,0)-\Upsilon,\Theta(x,0)-\Upsilon) \to \left(\widetilde{N}_\Upsilon(x,t),\tilde{\Theta}_\Upsilon(x,t)\right). \tag{30}$$

The pair $\left(\widehat{N}_\Upsilon(x,t),\hat{\Theta}_\Upsilon(x,t)\right)$ is formed of upper solutions that are time monotone nonincreasing while the pair $\left(\widetilde{N}(x,t),\tilde{\Theta}(x,t)\right)$ is formed of nondecreasing lower solutions for any $t>0$.

Given a $t>0$, it holds that:

$$\left(\widehat{N}_\Upsilon(x,t),\hat{\Theta}_\Upsilon(x,t)\right)\geqslant\left(\widetilde{N}_\Upsilon(x,t),\tilde{\Theta}_\Upsilon(x,t)\right), \tag{31}$$

with

$$\lim_{\Upsilon\to 0}\left(\widehat{N}_\Upsilon(x,t),\hat{\Theta}_\Upsilon(x,t)\right)=\left(\widehat{N}(x,t)_a,\hat{\Theta}(x,t)_a\right), \tag{32}$$

$$\lim_{\Upsilon\to 0}\left(\widetilde{N}_\Upsilon(x,t),\tilde{\Theta}_\Upsilon(x,t)\right)=\left(\widetilde{N}(x,t)_a,\tilde{\Theta}(x,t)_a\right). \tag{33}$$

In addition,

$$\widehat{N}(x,t)_a\geqslant\widetilde{N}(x,t)_a,\ \hat{\Theta}(x,t)_a\geqslant\tilde{\Theta}(x,t)_a. \tag{34}$$

Then, the pair of upper solutions $\left(\widehat{N}_a(x,t),\hat{\Theta}_a(x,t)\right)$ is timely nonincreasing and the pair of lower solutions $\left(\widetilde{N}_a(x,t),\tilde{\Theta}_a(x,t)\right)$ nondecreasing.

Proof. We first should discuss about the ordered conditions between the upper solutions and the lower solutions. This assessment follows from standard techniques (see Ch. 12 in the reference [24]):

$$\left(\widehat{N}_\Upsilon(x,t),\hat{\Theta}_\Upsilon(x,t)\right)\geqslant\left(\widetilde{N}_\Upsilon(x,t),\tilde{\Theta}_\Upsilon(x,t)\right). \tag{35}$$

The coming idea is to prove the monotone behaviour of each solution, $\widehat{N}_\Upsilon$, $\widetilde{N}_\Upsilon$, $\hat{\Theta}_\Upsilon$ and $\tilde{\Theta}_\Upsilon$. For this, consider two fixed positive real constants $\beta_1>0$ and $\beta_2>0$, such that:

$$\begin{aligned}&\widetilde{N}_{\Upsilon,\beta_1}(x,t)=\widetilde{N}_\Upsilon(x,t+\beta_1)-\widetilde{N}_\Upsilon(x,t);\ \tilde{\Theta}_{\Upsilon,\beta_1}(x,t)=\tilde{\Theta}_\Upsilon(x,t+\beta_1)-\tilde{\Theta}_\Upsilon(x,t)\\&\widehat{N}_{\Upsilon,\beta_2}(x,t)=\widehat{N}_\Upsilon(x,t+\beta_2)-\widehat{N}_\Upsilon(x,t);\ \hat{\Theta}_{\Upsilon,\beta_2}(x,t)=\hat{\Theta}_\Upsilon(x,t+\beta_2)-\hat{\Theta}_\Upsilon(x,t).\end{aligned} \tag{36}$$

As mentioned, we shall find a nondecreasing lower solution for N, then for any Υ:

$$\widetilde{N}_{\Upsilon,\beta_1}(x,t)=\widetilde{N}_\Upsilon(x,t+\beta_1)-\widetilde{N}_\Upsilon(x,t)\geqslant 0. \tag{37}$$

To continue the proof, we define the following parabolic operator for any positive function $\Sigma(x,t)\in C^{2+\alpha,\,1+\alpha/2}\left(\mathbb{R}^3\times(0,T)\right)$, $\alpha>0$:

$$\mathscr{L}\Sigma=\Sigma_t-\gamma\Delta\Sigma-a\cdot\nabla\Sigma, \tag{38}$$

where γ can be either δ or ϵ, as per the diffusion coefficients in (1).

The functions $\widehat{N}_{\Upsilon,\beta_2}$, $\widetilde{N}_{\Upsilon,\beta_1}$, $\hat{\Theta}_{\Upsilon,\beta_2}$ and $\tilde{\Theta}_{\Upsilon,\beta_1}$ verify the Eq. (1), so that the following holds:

$$\begin{aligned}&\mathscr{L}\left(\widetilde{N}_{\Upsilon,\beta_1}\right)=\tilde{\Theta}_\Upsilon(x,t+\beta_1)^n-\tilde{\Theta}_\Upsilon(x,t)^n,\\&\mathscr{L}\left(\tilde{\Theta}_{\Upsilon,\beta_1}\right)=\widehat{N}_\Upsilon(x,t)^m-\widehat{N}_\Upsilon(x,t+\beta_2)^m,\\&\mathscr{L}\left(\widehat{N}_{\Upsilon,\beta_2}\right)=\hat{\Theta}_\Upsilon(x,t+\beta_2)^n-\hat{\Theta}_\Upsilon(x,t)^n,\\&\mathscr{L}\left(\hat{\Theta}_{\Upsilon,\beta_2}\right)=\widetilde{N}_\Upsilon(x,t)^m-\widetilde{N}_\Upsilon(x,t+\beta_1)^m.\end{aligned} \tag{39}$$

As $\mathscr{L}\left(\hat{\Theta}_{\Upsilon,\beta_2}\right)=\widetilde{N}_\Upsilon(x,t)^m-\widetilde{N}_\Upsilon(x,t+\beta_1)^m$:

$$\mathscr{L}\left(\hat{\Theta}_{\Upsilon,\beta_2}\right)\leqslant 0\to\hat{\Theta}_\Upsilon(x,t+\beta_2)\leqslant\hat{\Theta}_\Upsilon(x,t). \tag{40}$$

As $\mathscr{L}\left(\widehat{N}_{\Upsilon,\beta_2}\right)=\hat{\Theta}_\Upsilon(x,t+\beta_2)^n-\hat{\Theta}_\Upsilon(x,t)^n$:

$$\mathscr{L}\left(\widehat{N}_{\Upsilon,\beta_2}\right)\leqslant 0\to\widehat{N}_{\Upsilon,\beta_2}\leqslant 0\to\widehat{N}_\Upsilon(x,t+\beta_2)\leqslant\widehat{N}_\Upsilon(x,t). \tag{41}$$

Proceeding similarly for $\mathscr{L}\left(\tilde{\Theta}_{\Upsilon,\beta_1}\right)=\widehat{N}_\Upsilon(x,t)^m-\widehat{N}_\Upsilon(x,t+\beta_2)^m$, it holds that:

$$\mathscr{L}\left(\tilde{\Theta}_{\Upsilon,\beta_1}\right)\geqslant 0\to\tilde{\Theta}_{\Upsilon,\beta_1}\geqslant 0\to\tilde{\Theta}_\Upsilon(x,t+\beta_1)\geqslant\tilde{\Theta}_\Upsilon(x,t). \tag{42}$$

We first considered $\widetilde{N}_{\Upsilon,\beta_1}(x,t)\geqslant 0$, leading to $\tilde{\Theta}_\Upsilon(x,t+\beta_1)^n\geqslant\tilde{\Theta}_\Upsilon(x,t)^n$. We have obtained a condition that complies with the initial assumption of $\widetilde{N}_{\Upsilon,\beta_1}(x,t)\geqslant 0$.

Based on the exposed arguments, we conclude that any upper solution is monotone nonincreasing, and that any lower solution is monotone nondecreasing as initially postulated.

The upper and lower solutions can apply for any arbitrary small $0<\Upsilon\to 0^+$. For any Υ, the monotone behaviour of the upper and lower solutions hold. This result, together with the condition of a bounded finite mass evolution under the parabolicity of $\mathscr{L}$, permit to define the following limit condition:

$$\lim_{\Upsilon\to 0}\left(\widehat{N}(x,t),\hat{\Theta}(x,t)\right)=\left(\widehat{N}(x,t)_a,\hat{\Theta}(x,t)_a\right), \tag{43}$$

$$\lim_{\Upsilon\to 0}\left(\widetilde{N}(x,t),\tilde{\Theta}(x,t)\right)=\left(\widetilde{N}(x,t)_a,\tilde{\Theta}(x,t)_a\right). \tag{44}$$

Furthermore, the above limit solutions preserve the ordering property for $\Upsilon\to 0$, then:

$$\begin{aligned}&\tilde{\Theta}_a(x,t+\beta_1)\geqslant\tilde{\Theta}_a(x,t),\\&\widetilde{N}_a(x,t+\beta_1)\geqslant\widetilde{N}_a(x,t),\\&\hat{\Theta}_a(x,t+\beta_2)\leqslant\hat{\Theta}(x,t),\\&\widehat{N}_a(x,t+\beta_2)\leqslant\widehat{N}(x,t).\end{aligned} \tag{45}$$

As a consequence of all the exposed, the pair of upper solutions $\left(\widehat{N}_a(x,t),\hat{\Theta}_a(x,t)\right)$ is monotone nonincreasing, while the pair of lower solutions $\left(\widetilde{N}_a(x,t),\tilde{\Theta}_a(x,t)\right)$ is monotone nondecreasing. In addition, and for $t>0$, it holds that: $\widehat{N}_a\geqslant\widetilde{N}_a$, $\hat{\Theta}_a\geqslant\tilde{\Theta}_a$.

End of proof.

According to the set of Eqs. (1), the reaction and absorption terms are considered as functions of the involved solutions. We search for flat solutions departing from the initial data $\widetilde{N}(x,0)=N(x,0)-\Upsilon$ and $\hat{\Theta}(x,0)=\Theta(x,0)+\Upsilon$. Recall that r can be chosen so that $r-N=1$ and that $0<\Theta<1$, then the following problem can be study to predict the behaviour of flat upper and lower solutions:

$$\begin{aligned}&\widetilde{N}_t=\tilde{\Theta}^n,\quad\hat{\Theta}_t=-\widetilde{N}^m,\\&\widetilde{N}(x,0)=N(x,0)-\Upsilon,\quad\hat{\Theta}(x,0)=\Theta(x,0)+\Upsilon.\end{aligned} \tag{46}$$

It should be noted that any solution to the last problem shall comply with the results related with the monotone behaviour of solutions in (45).

In order to provide solutions for the problem (46), we should make a hypothesis for the lower solution $\tilde{\Theta}$. For this purpose, assume that it is possible to know beforehand the lowest or terminal threshold of oxygen concentration (in fact this is a soft assumption as such a oxygen concentration is known from the literature, see for example [22]). Then a solutions is: (see Figs. 1 and 2)

$$\tilde{\Theta} = \theta^{1/n}. \tag{47}$$

The problem (46) reads:

$$\begin{aligned} \widetilde{N}_t = \theta, \quad \hat{\Theta}_t = -\widetilde{N}^m, \\ \widetilde{N}(x,0) = N(x,0) - \Upsilon, \quad \hat{\Theta}(x,0) = \Theta(x,0) + \Upsilon. \end{aligned} \tag{48}$$

After solving with simple standard techniques, the following solutions are obtained:

$$\begin{aligned} \widetilde{N}(t) = \widetilde{N}_0 + \theta t, \\ \hat{\Theta}(t) = \hat{\Theta}_0 - \tfrac{1}{\theta(m+1)}\left(\widetilde{N}_0 + \theta t\right)^{m+1}. \end{aligned} \tag{49}$$

Given the finite mass initial distribution, one has:

$$\|\widetilde{N}_0\|_{L^1} = \|N(x,0)\|_{L^1} - \Upsilon_n. \tag{50}$$

For Θ:

$$\|\hat{\Theta}_0\|_{L^1} = \|\Theta(x,0)\|_{L^1} + \Upsilon_n. \tag{51}$$

The constant Υ_n may be different from Υ and is introduced to make the equality in the Schwarz inequality, then:

$$\|N(x,0) - \Upsilon\|_{L^1} = \|N(x,0)\|_{L^1} - \Upsilon_n \leqslant \|N(x,0)\|_{L^1} + \Upsilon. \tag{52}$$

For Θ:

$$\|\Theta(x,0) + \Upsilon\|_{L^1} = \|\Theta(x,0)\|_{L^1} + \Upsilon_n \leqslant \|\Theta(x,0)\|_{L^1} + \Upsilon, \tag{53}$$

We can make $\Upsilon_n \to 0$ (similarly for Υ), so that the resulting solutions are given as:

$$\begin{aligned} \widetilde{N}_a(t) = \|N(x,0)\|_{L^1} + \theta t, \\ \hat{\Theta}_a(t) = \|\Theta(x,0)\|_{L^1} - \tfrac{1}{\theta(m+1)}(\|N(x,0)\|_{L^1} + \theta t)^{m+1}. \end{aligned} \tag{54}$$

It should be mentioned that the solutions preserve the monotone behaviour within a time interval $(0, T)$. Such a value of T can be obtained as:

$$\theta^{1/n} = \|\Theta(x,0)\|_{L^1} - \frac{1}{\theta(m+1)}(\|N(x,0)\|_{L^1} + \theta T)^{m+1}, \tag{55}$$

$$T = \frac{(\theta(m+1))^{\frac{1}{m+1}}\left(\|\Theta(x,0)\|_{L^1} - \theta^{1/n}\right)^{\frac{1}{m+1}} - \|N(x,0)\|_{L^1}}{\theta}. \tag{56}$$

Assuming that $\|\Theta(x,0)\|_{L^1} \gg \theta^{1/n}$, the monotone property of solutions is preserved provided that:

$$\theta(m+1)\left(\|\Theta(x,0)\|_{L^1} \geqslant \|N(x,0)\|_{L^1}^{m+1}. \right. \tag{57}$$

So that a value for θ is obtained as:

$$\theta \geqslant \frac{\|N(x,0)\|_{L^1}^{m+1}}{(m+1)\|\Theta(x,0)\|_{L^1}}. \tag{58}$$

Once the flat solutions have been obtained, supported by an argument related with their monotone behaviour, it is the intention to determine particular values for the involved constants and the existence time T. Again, the flight test data for this purpose comes from the reference [22] (see the Fig. 3).

Note that the second solution in (3) is partly modified to account for a scaling constant K to be assessed:

$$\hat{\Theta}_a(t) = \|\Theta(x,0)\|_{L^1} - \frac{K}{\theta(m+1)}(\|N(x,0)\|_{L^1} + \theta t)^{m+1}. \tag{59}$$

For the coming argument, recall that the terminal level of oxygen concentration is given as $\hat{\Theta} = \theta^{\frac{1}{n}}$. Such a value can be obtained based on the data from Fig. 3. Previously, we should mention that, in case the stabilized cruising phase would have continued further, the oxygen concentration may have gone down to the 2% level. To show this, it suffices to check the curvature of the graph in Fig. 3 and close to $t = 70$ min. In addition, the terminal level of 2% is well-known to hold based on experimental findings. The reader is referred to the studies [22,3,4] for further scientific reasoning. Note that the oxygen concentration grows suddenly due to the starting of the descend phase, in which the oxygen enriched air in the atmosphere goes inside the tank through the tank venting system. Considering such a minimum level of oxygen concentration $\hat{\Theta} = 0.02$, we have that $\theta = 0.1$.

Hence, the following solutions hold:

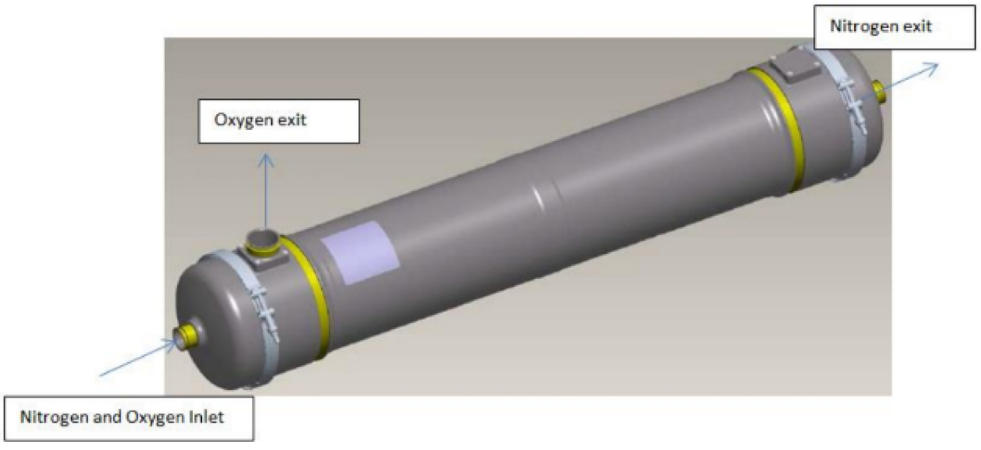

Fig. 1 Air Separation Module (ASM) external shape.

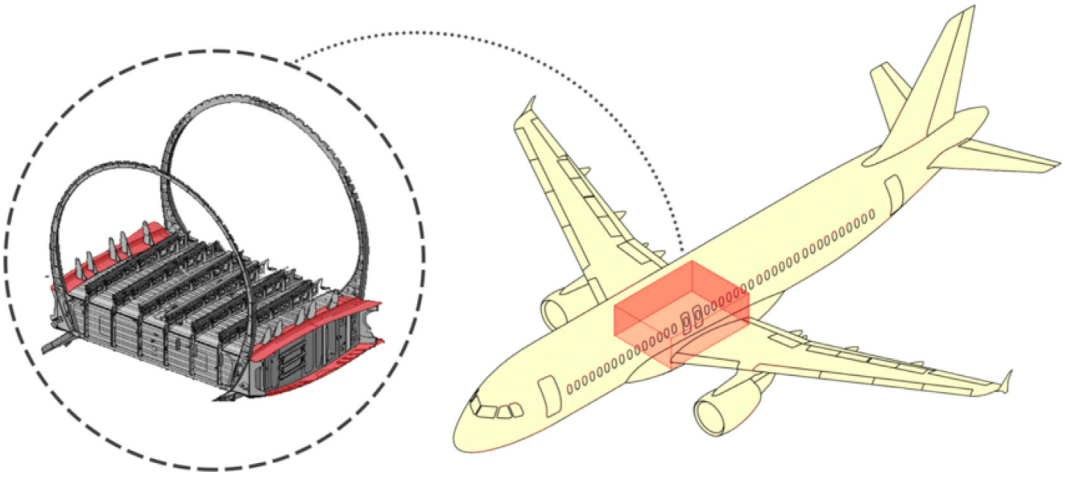

Fig. 2 General sketch of the A320 Centre Wing Box (Source reference [23]).

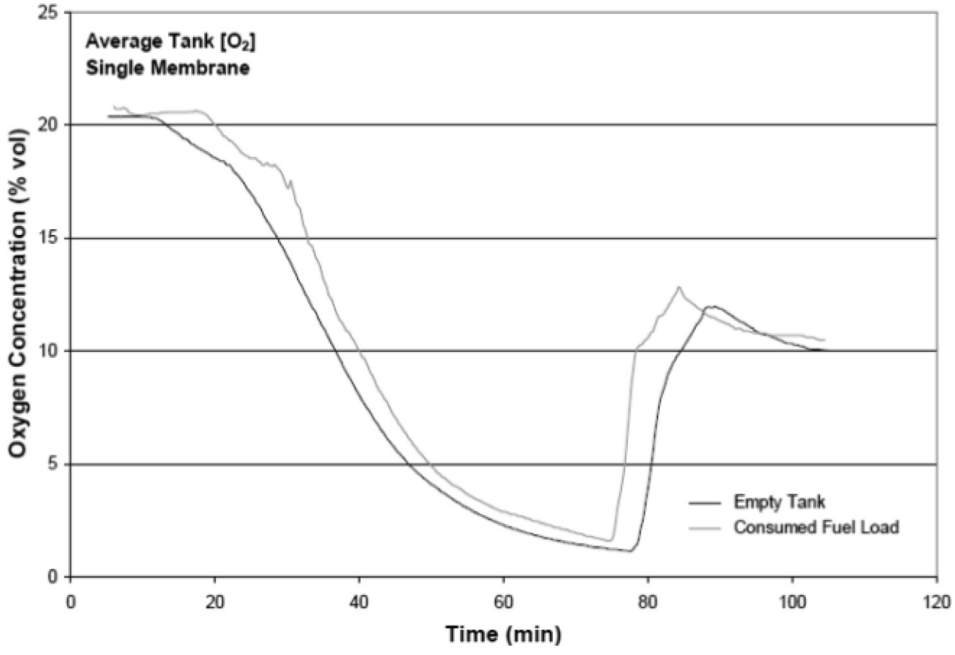

Fig. 3 Oxygen concentration for empty tanks and one ASM working. (Source reference is [22]).

$$\begin{aligned} \widetilde{N}_a(t) &= 0.8 + 0.1t, \\ \hat{\Theta}_a(t) &= 0.2 - K9.75\,(0.8 + 0.1t)^{1.025}. \end{aligned} \tag{60}$$

The constant K was introduced as a calibrating parameter, and to make the involved magnitudes dimensions compatible. Hence it suffices to consider a single flight test point, as coming from Fig. 3, for an assessment of such K. We choose the point $t = 40$ min, for which the oxygen concentration level is of 0.08. Any other point can be considered as well with negligible differences in the value of K, nonetheless we have preferred to select the point at $t = 40$ min, as it is a mid point where the flight is stabilized, and the decreasing rate is higher compared to other zones. After standard operation in (60), the following value is obtained:

$$K = 2.465 \cdot 10^{-3}. \tag{61}$$

The time, for which the postulated solutions holds, is assessed based on the expression (56):

$$|\,T\,| = 7.801 \text{ seconds} = 0.130 \text{ min}\,. \tag{62}$$

Therefore, the solutions hold in time steps of amplitude 7.801 seconds. In order to make an application of the obtained solutions to a complete flight profile, the time shall be discretized in intervals of maximum 7.801 seconds, so as to preserve the minimality of the lower solution $\widetilde{N}_a(t)$, and the maximality of the upper solution $\hat{\Theta}_a(t)$. The Fig. 4 provides the graph of the oxygen solution in (60) compared to the real flight test values obtained from the Fig. 3.

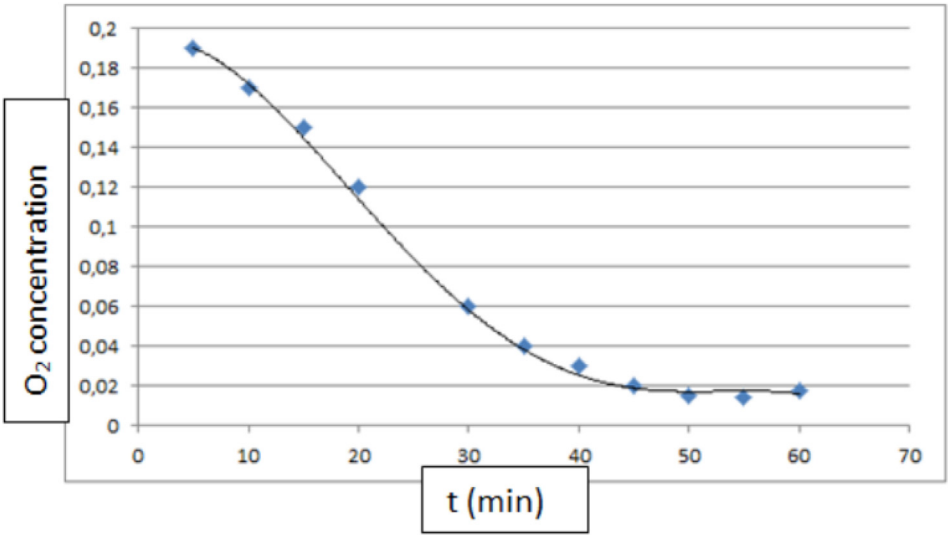

Fig. 4 The black graph is the representation of the oxygen solution in (60), after having performed a time discretization of amplitude 7.801 seconds. The blue discrete points are obtained from the Fig. 3. The solution under (60) evolves closely to the real flight test data. The initial condition in each time step is given by the final condition in the previous step. This permits to increase the accuracy of the fitting process followed.

6. Conclusions

The initial objectives withdrawn have been tracked in the set of analysis provided. The model proposed in (1) considered the three main physical principles given in any gas interaction in a fuel tank, namely; diffusion, vented convection and reaction/absorption. These represent the most remarkable advantage of the model (1), that is formulated based on a physical interpretation of diffusion (as the interaction between the gas particles), the advection (as the forced convection because of the action of the tank ventilation ourboard) and the reaction (as the entering gas into the tank through dedicated nozzles). In the presented analysis, we introduced a novel approach, consisting in establishing the required compatibility conditions, about the relative importance among the mentioned physical principles. Indeed, if the vented convection is predominant over the other terms, the injected nitrogen would not reach all the tank locations, as the convection would transport such nitrogen to the venting outlet. Under this condition, no inerted ullage can be achieved. In the present study (see Theorem 1), we have shown that this is not the case: The reaction term, related with the nitrogen injection, is predominant over the vented convection. In addition, a compatibility result has been obtained to ensure that the diffusion is predominant over the advection term. This is important for zones of a difficult geometry, where the air at stagnation makes the nitrogen to move by diffusion. In addition, we have obtained flat solutions to the problem (1). The flat solutions constituted a novelty to ease the process for assessing a time-to-inert in a tank. Both the compatibility results and the flat solutions obtained, have been validated with real flight test data to show the applicability scope of our results.

As future research topics related with the proposed model, we consider that a complete set of computational and analytical techniques can be put in place to continue exploring the model. In particular, to study the stationary distributions for (1) (this is solutions of the form $N(x, t = \tau) = N(x)$, $\Theta(x, t = \tau) = \Theta(x)$, for a fixed τ), we can use a Quasilinearization method to the resulting ODE system (refer to [25] for a wide discussion and application about this method). From an analytical perspective, the use of the Pi-Buckingham theorem could help us to reduce the modelling complexity (see the reference [26] for an application to a complex Casson fluid). In addition, we can extend the idea of diffusion by exploring nonlocal operators, that have been previously used with success to explore the modeling exercises in material sciences (see [27] for the thermoelastic theory, for which the form of the equations can be used in fluid modeling and, by hypothesis, in our model).

Declaration of Competing Interest

The authors declare that they have no known competing financial interests or personal relationships that could have appeared to influence the work reported in this paper.

References

[1] FAA. Advisory Circular Ref. 25.981-1C. Fuel Tank Ignition Source Prevention Guidelines.
[2] Aircraft Accident Report. National Transportation Safety Board ref NTSB/AAR-00/03.
[3] M. Burns, W. Cavage, Inerting of a vented aircraft fuel tank test article with nitrogen enriched air. Report no. DOT/FAA/AR-01/6, 2001.
[4] W. Cavage, T. Bowman, Modeling in flight inert gas distribution in a 747 center wing fuel tank, in: 35th AIAA fluid dynamics conference and exhibit. Canada, 2005.
[5] Y. Wei, Y. Pei, Y. Ge, Analytical Algorithm for Oxygen Concentration of Aircraft Fuel Tank in Various Inerting Stages, Appl. Sci. 11 (2021) 7698, https://doi.org/10.3390/app11167698.
[6] E. Ghadirian, J. Brown, S. Wahiduzzaman, A quasy-steady diffusion based model for design and analysis of fuel tank

evaporate emissions, SAE Technical Paper ref. 2019–01-0947 (2019).
[7] L. Shao, W. Liu, C. Li, S. Feng, C. Wang, Pan, J. Experimental comparison between aircraft fuel tank inerting processes using NEA and MIG, Chin. J. Aeronaut. 31 (2018) 1515–1524.
[8] L. Shao, W. Liu, C. Li, S. Feng, B. Sun, Pan, J. Experimental Comparison of Fuel Scrubbing Inerting Process Using Nitrogen and Carbon Dioxide of Aircraft Fuel Tanks, Fire Technol. 54 (2017) 379–394.
[9] K.S. Bae, E.L. Blosch, Outgassing Characteristics from Oxygen Dissolved in JP-8 during Depressurization, J. Propuls. Power 36 (2020) 446–452.
[10] Summer, S. (2003). Limiting Oxygen Concentration Required to Inert Jet Fuel Vapors Existing at Reduced Fuel Tank Pressures. FAA Report Number: DOT/FAA/AR-TN02/79.
[11] Y. Pei, B. Shi, Method for analyzing the effect of projectile impact on aircraft fuel tank inerting for survivability design. Proc. Inst, Mech. Eng. Part G J. Aerosp. Eng. 230 (2016) 2345–2355.
[12] L. Shao, S. Feng, C. Li, W. Liu, X. Huang, Effect of scrubbing efficiency on fuel scrubbing inerting for aircraft fuel tanks, Aircr. Eng. Aerosp. Technol. 91 (2019) 225–234.
[13] S. Feng, C. Li, X. Peng, T. Wen, Y. Yan, R. Jiang, W. Liu, Oxygen concentration variation in ullage influenced by dissolved oxygen evolution, Chin. J. Aeronaut. 33 (2020) 1919–1928.
[14] Liu, D.J. (2014). Numerical Study of the Influence of Ambient Pressure on the Inerting Effect of an Aircraft Fuel Tank Inerting System. Advanced Materials Research (Vols. 1061–1062, pp. 1140–1143). Trans Tech Publications, Ltd. doi: 10.4028/www.scientific.net/amr.1061-1062.1140.
[15] J.L.D. Palencia, Travelling Waves Approach in a Parabolic Coupled System for Modelling the Behaviour of Substances in a Fuel Tank, Appl. Sci. 11 (2021) 5846, https://doi.org/10.3390/app11135846.
[16] M. Daigle, V. Smelyanskiy, J. Boschee, M. Foygel, Temperature Stratification in a Cryogenic Fuel Tank, Journal of Thermophysics and Heat Transfer. 27 (1) (2013) 116–126, https://arc.aiaa.org/doi/abs/10.2514/1.T3933.
[17] K. Kinefuchi, Y. Umemura, Numerical Study of Effect of Pressurant Gas Species on Thermal Behavior in Cryogenic Tank, Journal of Spacecraft and Rockets 59 (4) (2022) 1262–1275, https://arc.aiaa.org/doi/abs/10.2514/1.A35061.
[18] E. Anderson, S. Chintalapati, D. Kirk, Modeling of Ullage Collapse Within Rocket Propellant Tanks at Reduced Gravity, Journal of Spacecraft and Rockets. 51 (5) (2014) 1377–1389, https://arc.aiaa.org/doi/abs/10.2514/1.A32308.
[19] V. Singal, J. Bajaj, N. Awalgaonkar, S. Tibdewal, CFD Analysis of a Kerosene Fuel Tank to Reduce Liquid Sloshing, Procedia Engineering 69 (2014) 1365–1371, https://doi.org/10.1016/j.proeng.2014.03.130.
[20] L. Er, Z. Xiangying, Evaluating the performance of fine bubble diffused aeration systems in cylindrical aeration tanks by fuzzy c-means algorithm, Water Science and Technology. 84 (2) (2021) 404–419.
[21] X. Xi, H. Liu, C. Cai, M. Jia, H. Yin, Analytical Study on Homogeneous Nucleation and Bubble Evolution Inside Monocomponent Fuel Droplet, Journal of Thermophysics and Heat Transfer. 35 (3) (2021) 560–568, https://arc.aiaa.org/doi/abs/10.2514/1.T6155.
[22] Flight-Testing of the FAA Onboard Inert Gas Generation System on an Airbus A320. DOT/FAA/AR-03/58.
[23] Mena Andrade, Ramiro Aguado, Jose V. Guinard, Stéphane Huerta, Antonio, Reshaping diagrams for bending straightening of forged aeronautical components, International Journal of Advanced MaUpsilonfacturing Technology. 110 (2020), https://doi.org/10.1007/s00170-020-05856-z.
[24] C. Pao, Nonlinear Parabolic and Elliptic Equations, Springer Science, 2012.
[25] S. Khan, F. Ali, W.A. Khan, et al, Quasilinearization numerical technique for dual slip MHD Newtonian fluid flow with entropy generation in thermally dissipating flow above a thin needle, Sci Rep 11 (2021) 15130, https://doi.org/10.1038/s41598-021-94312-3.
[26] N. Ahmad Sheikh, D. Ling Chuan Ching, T. Abdeljawad, I. Khan, M. Jamil, et al, A fractal-fractional model for the mhd flow of casson fluid in a channel, Computers, Materials Continua 67 (2) (2022) 1385–1398.
[27] Aatef Hobiny, Ibrahim A. Abbas, A study on the thermoelastic interaction in two-dimension orthotropic materials under the fractional derivative model, Alexandria Eng. J. (2022), https://doi.org/10.1016/j.aej.2022.08.047.